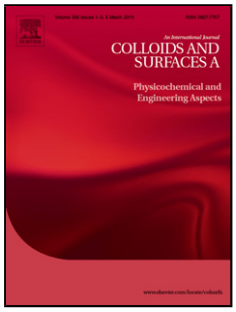

Title: Hydration induced morphological change on proppant surfaces employing a calcium-silicate cement system

Authors: Covadonga Correas, Kourtney Wright, Enrico Andreoli, Zeyad Almutairi, Bjornar Sandnes, Andrew R. Barron

PII: S0927-7757(17)30898-1
DOI: https://doi.org/10.1016/j.colsurfa.2017.10.006
Reference: COLSUA 21964

To appear in: *Colloids and Surfaces A: Physicochem. Eng. Aspects*

Received date: 11-8-2017
Revised date: 4-10-2017
Accepted date: 5-10-2017

Please cite this article as: Covadonga Correas, Kourtney Wright, Enrico Andreoli, Zeyad Almutairi, Bjornar Sandnes, Andrew R.Barron, Hydration induced morphological change on proppant surfaces employing a calcium-silicate cement system, Colloids and Surfaces A: Physicochemical and Engineering Aspects https://doi.org/10.1016/j.colsurfa.2017.10.006

Submitted to *Colloids Surf., A.*

Hydration induced morphological change on proppant surfaces employing a calcium-silicate cement system

Covadonga Correas,[a] Kourtney Wright,[b] Enrico Andreoli,[a] Zeyad Almutairi,[c,d,e] Bjornar Sandnes,[a] Andrew R. Barron[a,b,f]*

[a] *Energy Safety Research Institute, Swansea University Bay Campus, Swansea, SA1 8QQ, Wales, United Kingdom*

[b] *Department of Chemistry, Rice University, Houston, TX 77005, USA.*

[c] *Department of Mechanical Engineering, King Saud University, Riyadh 11421, Saudi Arabia.*

[d] *Sustainable Energy Technology Center, King Saud University, Riyadh 11421, Saudi Arabia.*

[e] *King Abdullah Institute of Nanotechnology, King Saud University, Riyadh 11421, Saudi Arabia.*

[f] *Department of Materials Science and Nanoengineering, Rice University, Houston, TX 77005, USA.*

*Corresponding author.

E-mail addresses: a.r.barron@swansea.ac.uk; arb@rice.edu (A. R. Barron)

Graphical abstract

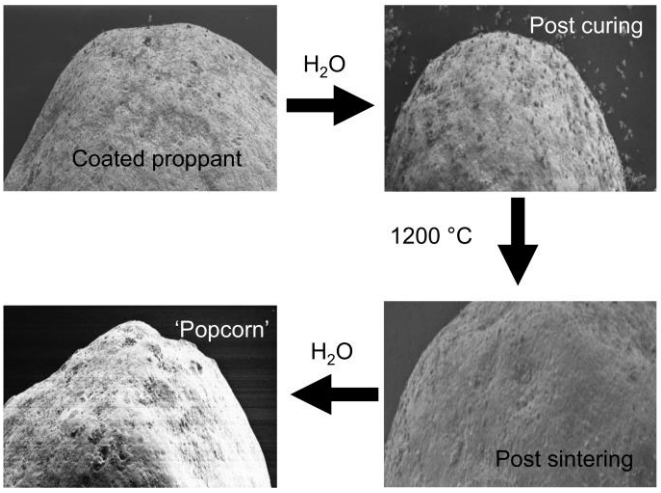

Submitted to *Colloids Surf., A.*

Highlights

- Proppant particles have been coated with Ca-Si oxides.
- Si reagents during the synthesis increase the particle size and the adherence of the coatings to the proppant.
- Hydration provides an in-situ increase in the angularity to immobilize the proppant.

ABSTRACT Commercial aluminosilicate proppant particles have been coated with Ca-Si oxides, with the aim to provide an in-situ increase in the angularity (decrease in Krumbein roundness value) to facilitate their immobilization. Ca-Si oxide systems have been synthesized via sol-gel, cured, and sintered at 1200 °C using (a) $CaCO_3$, (b) $CaCO_3$ + orthosilicic acid ($Si(OH)_4$, SA), and (c) $CaCO_3$ + fused silica (SiO_2, FS). When the proppant is cured in the presence of $CaCO_3$ and silicic acid the coatings undergo a significant compositional change, while sintering results in the conversion of the cured samples to ceramic agglomerates with the desired "popcorn" shapes. The best results are obtained in the presence of Si reagents, and hydration of these sintered proppants allows for a distinct increase in the angularity, which is the desired transformation to allow the proppant to be locked-in-place once located in the reservoir. The samples have been characterized at each stages of preparation by scanning electron microscopy (SEM) with associated energy dispersive X-ray spectroscopy (EDX), X-ray photoelectron spectroscopy (XPS), X-rad diffraction (XRD) and infrared (IR) spectroscopy.

Keywords: Proppant, $CaCO_3$, cement, fumed silica, orthosilicic acid, calcium silicate cement

Submitted to *Colloids Surf., A.*

1. Introduction

With a reserve estimated at 482 trillion cubic feet (Tcf) of hydrocarbon, shale gas has the potential to be the primary energy source for power generation in the US for the coming decades [1]. The ability to extract shale oil and gas economically has been enabled achieved by the development of hydraulic fracturing along with horizontal drilling techniques [2]. Hydraulic fracturing (also known as “fracing” or “fracking”) uses water, a proppant, and various chemical additives pumped at high pressures into the well bore, to induce fracturing of the impermeable shale source rock, creating sufficient permeability for the gas to migrate into the well bore and from there to the surface [3-5]. During this process a proppant material is used to “prop” open the fractures, stabilizing the well and allowing the gas to escape once the pressure is removed. These proppant materials need to be sufficiently hard to withstand the stress upon removal of the pressurized fluid. In addition, it is desirable that they are of uniform size and shape to enhance the flux of the oil, natural gas and natural gas liquids out of the rock formations [6].

Most proppant consists of sand, made from high purity sandstone; however, alternative ceramic particles made from sintered bauxite are used [7]. The proppant must be mobile enough in the fluid to be introduced into the fractures in the rocks during the pumping of high-pressure water based fluid in the stimulation process. However, once in place the proppant should not be mobile. Unfortunately, the proppant can unintentionally shift from the desired location in the well formation, and the subsequent loss of proppant is a leading cause of production decline. Counter to this situation, if the proppant is insufficiently mobile then only a fraction of the fracture can be propped since the proppant will create a bridge prior to the tip of the fracture. Attempts to address this problem using elongated shapes or other specific non-spherical materials have not been successful since a non-spherical shape is more difficult to pump. What is needed is a proppant that is non-aggregated during pumping, but is then aggregated or immobilized downhole without loss in permeability. To this end several methods have been investigated, including: coating proppant with liquid surface-modification agent (SMA) resins [8], oligomers of furfuryl alcohol resin [9], various adhesive substances

[10], organo-silanes [11], thermoplastic resins [12], immobilization via molecular anchors [13,14] and microwave irradiation [15]. An alternative route would be a spherical proppant that once in place "cures" to create a lock-and-key interaction via a morphological change on proppant surfaces (Fig. 1).

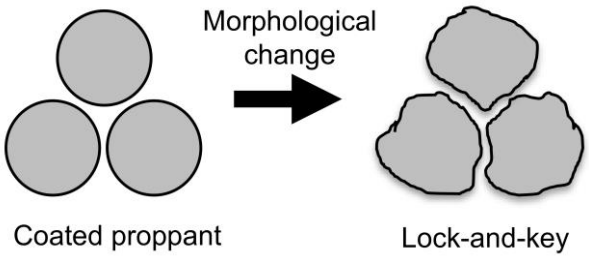

Fig. 1. Schematic representation of a post placement morphological change on proppant surfaces to create an interlock to immobilize the proppant.

We have previously shown that, in the presence of a calcium binding agent, $CaCO_3$ may undergo a surface reorganization [16]; however, such a process would require the use of additional chemical, when public pressure is to limit chemicals employed downhole [5,17]. In contrast, Portland cement represents a material that under mild conditions (hydration) undergoes reactions that result in morphological change as well as fusing individual grains together [18]. Furthermore, the hardness of set cement would be suitable for a proppant material once in place [19]. Given that typical ceramic proppants are aluminosilicate then the potential inclusion of a calcium source could produce one or more of the cement main phases: tricalcium silicate ($3CaO\text{-}SiO_2$), dicalcium silicate ($2CaO\text{-}SiO_2$), and tricalcium aluminate ($3CaO\text{-}Al_2O_3$) [20,21]. Herein, we have investigated the surface reaction of a typical commercial aluminosilicate proppant with $CaCO_3$ (including at high temperature) and its subsequent hydration to determine if any suitable surface morphological change occurs through reaction with the templating alumino silicate proppant. The known interaction of fumed silica with cement materials [22] and our prior report [23], which has shown that the reaction of $CaCO_3$ with either orthosilicic acid ($Si(OH)_4$, SA) or fused silica (SiO_2, FS) can create distinctive nodular morphology under mild conditions, would suggest that a

combination of both $CaCO_3$ with a silica source would offer the ability to react on the surface of the proppant forming a calcium silicate cement (CSC). Such materials have been proposed as fast setting bone cements [24]. A representation of the procedures used herein is shown in Fig. 2.

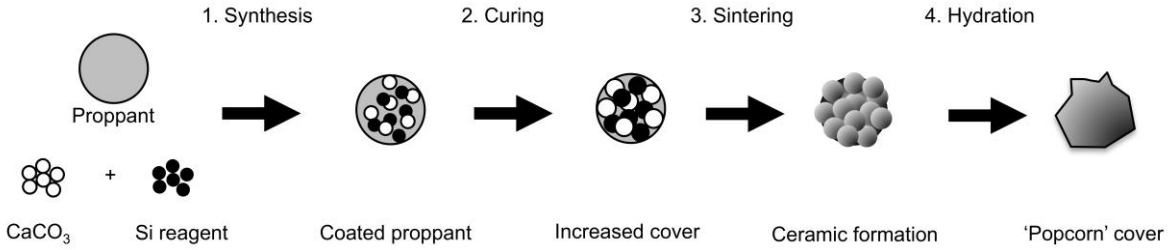

Fig. 2. Schematic illustration of the preparation procedure used in the present study showing (i) the reaction of an alumina silicate proppant with $CaCO_3$ and a silicon containing reagent to form a coating on the proppant; (ii) curing this product by the addition of distilled water for 1 week results in increased cover of the proppant surface, (iii) sintering the cured coating to 1200 °C results in new phase formation, and (iv) undergoes a morphological change upon hydration.

2. Materials and Methods

2.1. Materials

ACS grade calcium carbonate ($CaCO_3$, Cal), orthosilicic acid [$Si(OH)_4$, SA], and fumed silica (SiO_2, FS) were purchased from Sigma Aldrich and used as received. Deionised (DI) water (Mallinckrodt chemical works). Carbon dioxide was 99.99% pure, Matheson TRIGAS. The proppant (P) was obtained from CARBO Ceramics, Inc., and has a main composition of aluminosilicate, a range of particle size of 60-700 μm (average size = 370 μm), and a density of 1.57 g/cm^3.

2.2 Sample preparation

A summary of the reagent combinations and the sample abbreviations is given in Table 1. Samples with and without proppant were processed in a near identical manner (except for the presence or absence of proppant), the only difference being the relative water quantities

employed. In all the cases solid $CaCO_3$ (500 mg) was added to deionised water (250 mL) and stirred at ambient pressure under a flow of CO_2 for 1 hour (5 hours in the case of just $CaCO_3$ as reagent, i.e., Cal). In the experiments with proppant, 4.0 g of proppant were employed. Where used (Table 1), 50 mg of either orthosilicic acid (SA) or fumed silica (FS) was added, while stirring and bubbling with CO_2 for 4 hours. After this time, the reaction was kept under a CO_2 atmosphere with continuous stirring for 20 hours. Finally, the samples were filtered by gravity and dried in an oven at 70 °C for 1 hour to be characterized before the curing process. The samples with proppant were sieved (70 mesh = 0.212 mm) after drying, keeping the coated proppant (retained by the sieve) and the excess powder (passed through the sieve) separated. It should be noted that 'excess powder' refers to the powder that is formed from the proppant surface due to physical handling of the proppant, in contrast 'powder' is used to describe material formed in the absence of proppant.

The curing process was performed by adding distilled water to small amounts of sample and aging for 1 week under ambient indoor conditions (*ca*. 20 °C, 1 atm). The samples with proppant were cured after having added back a small amount of excess powder to the proppant. After 1 week, most of the water was removed and the samples were dried in an oven at 70 °C for 1 hour. In order to test for the effect of cure time, the sample synthesized using calcium carbonate and orthosilicic acid (Cal-SA-P) was also cured for 2 months under ambient indoor conditions. The cured and dried samples were sintered by heating from room temperature to 1200 °C in air, at a rate of 10 °C/min, followed by 1.5 h isotherm at the highest temperature and natural cooling. The samples with proppant were obtained from the heating of coated proppant with a large amount of excess powder. Sintered samples were subsequently hydrated by exposure to water for 48 h.

Submitted to *Colloids Surf., A.*

Table 1

Summary of sample combinations.

Sample abbreviation*	$CaCO_3$ (mg)	$Si(OH)_4$ (mg)	SiO_2 (mg)	Proppant (g)
Ca	500			
Ca-P	500			4.0
Ca-SA	500	50		
Ca-SA-P	500	50		4.0
Ca-FS	500		50	
Ca-FS-P	500		50	4.0

* Reagent abbreviations: Ca = $CaCO_3$; SA = $Si(OH)_4$; FS = SiO_2; P= proppant.

2.3. Characterization methods

The crystallographic structure of the products has been investigated by XRD with a Bruker AXS D8 Advance diffractometer with an LINXEYE detector between 10° and 70° (2θ), with 2θ increments of 0.02° and counting time of 0.5 s. The Cu-K_α (λ=1.5418 Å) was used in these experiments. Thermoscientific i510 ATR-FTIR was used to carry out the IR analysis of all the samples, recording spectra in the 650-4000 cm^{-1} region with 16 scans. XPS was preformed on a PHI Quantera system with a 1486.7 eV aluminum X-ray source. All spectra were recorded using a charge neutralizer to limit differential charging and subsequently calibrated to the carbon peak at a binding energy of 284.8 eV. Survey scans were recorded at a pass energy of 140 eV and high-resolution data at a pass energy of 26 eV. Data was fitted using MultiPak software. Thermogravimetric/differential thermal analysis (TG/DTA) of the samples were performed with a TA Q600 instrument, under flowing N_2 (100 mL/min) from room temperature to 1300 °C with a heating rate of 20 °C/min. The morphology of the powder, excess powder, and proppant samples was examined by field emission scanning electron microscopy using an Ultra-High Resolution FE-SEM S-4800, equipped with an Inca electron dispersive X-ray detector (Oxford Instruments, Abingdon, United Kingdom) for EDX experiments.

3. Results and Discussion

3.1. Synthesis

The syntheses consisted in mixing the reagents in deionised water under CO_2 atmosphere followed by filtering and drying of the collected products. Three different reagent combinations were used in order to examine enhancements in the proppant coating process: $CaCO_3$ alone as a reference and $CaCO_3$ with salicylic acid (SA, $Si(OH)_4$), and $CaCO_3$ with fumed silica (FS, SiO_2). Each of the three combinations was carried out either *with* or *without* proppant for a total of six different types of synthesis, as summarised with corresponding abbreviations in Table 1. Since it was observed that the physical agitation of the proppant samples during the coating reaction resulted in some of the coating being dislodged, this 'excess powder' was collected as a representative composition of the coating. Coated proppant and excess powder were separated using a sieve; however, the abbreviations Cal-P, Cal-SA-P and Cal-FS-P are used interchangeably to either refer to coated proppant particles or to their corresponding excess powder. These dislodged surface materials were compared to analogous reaction products formed in the absence of proppant, i.e., Cal, Cal-SA, and Cal-FS (Table 1), which were collected as dry 'powder'.

From SEM images it is apparent that the morphology of the coated proppants (Fig. 3b-d) is macroscopically similar to the untreated sample (Fig. 3a). From a comparison of the surfaces, it is evident that the modified proppants were, (i) covered with a homogeneous, rough and compact coating, (ii) the morphology of the coating is different than that of the surface of pristine proppant, and (iii) some small agglomerated were included in the coating. EDX mapping of the coatings (Fig. 4) indicate that the composition is relatively uniform. Thus, Ca is present across the sample, and the Si content is also relatively uniform. However, upon closer inspection of the surface it is clear that the films are not homogeneous. For example, the EDX analysis of Cal-FS-P revealed that the Si:Ca atomic ratio in the agglomerates was ca. 10, but it increased ca. 20 in the 'flat' areas surrounding the agglomerates. This is consistent with a model in which the surface of the proppant was covered with amorphous SiO_2 that acts as an adhesive for particles richer in Ca. Support for this hypothesis comes

from prior reports that SiO_2 tends to grow as an amorphous phase on Al_2O_3 surfaces and that $CaCO_3$ can be grown on amorphous silica surfaces [25, 26].

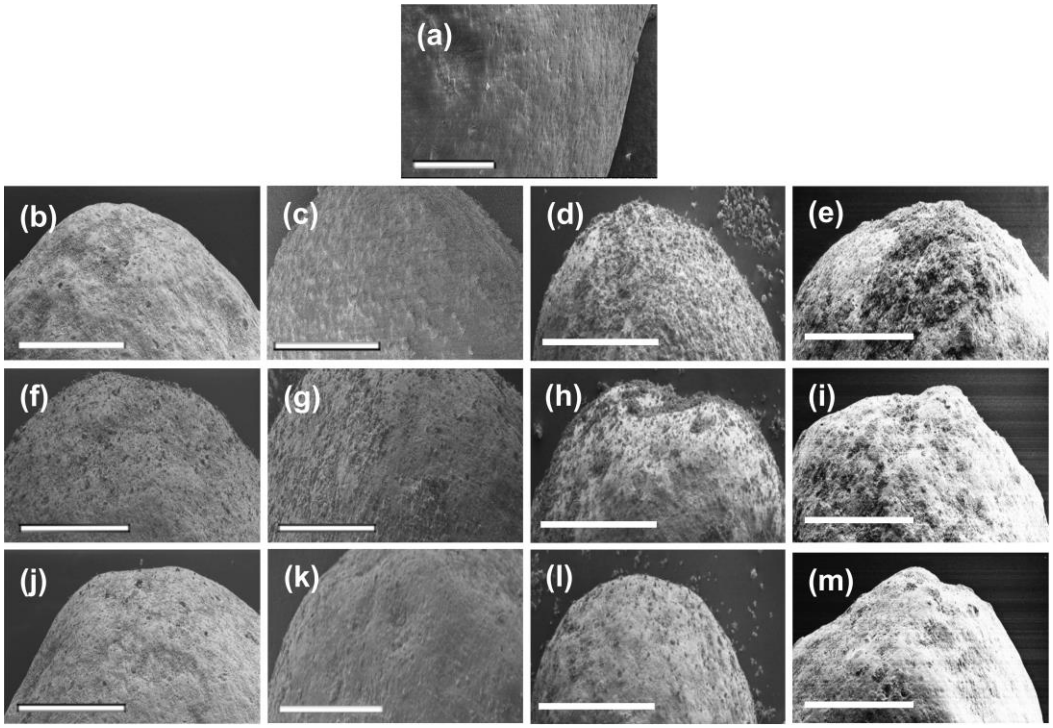

Fig. 3. SEM images of (a) a pristine proppant particle, and coated proppant particles from samples Cal-P, Cal-SA-P and Cal-FS-P obtained (b, f, j) after synthesis, (c, g, k) after curing, (d, h, l) after sintering and (e, I, m) after hydration, respectively. Scale bar is 300 μm in all images except for (a) where it is 200 μm.

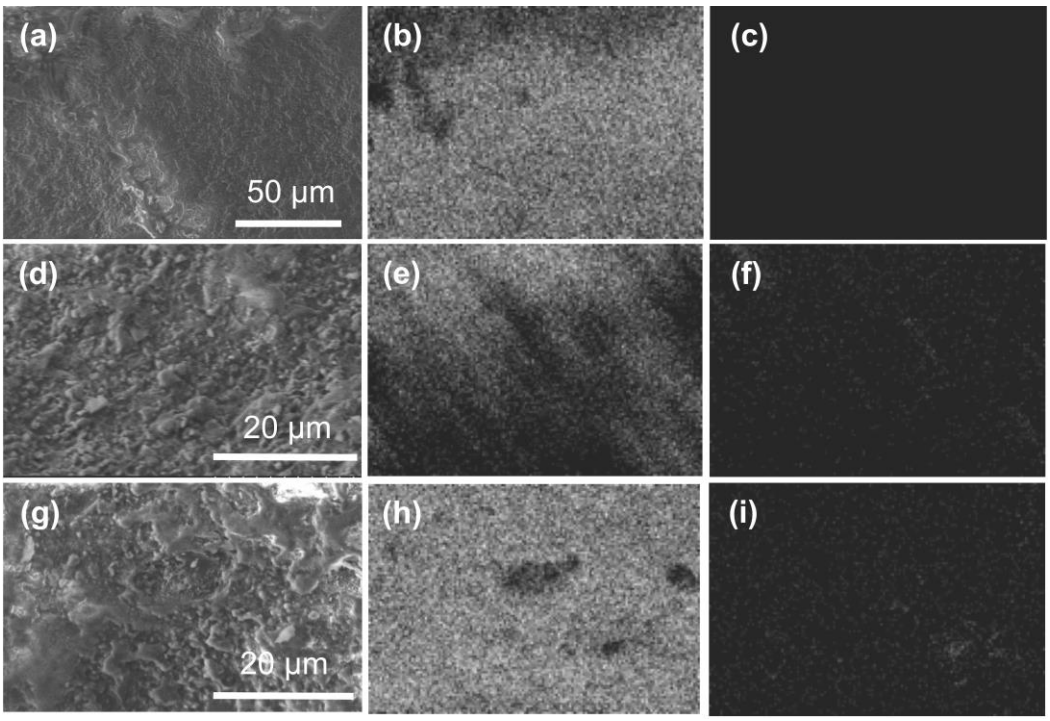

Fig. 4. The SEM images (a-c) and associated Ca (d-f) and Si (g-i) elemental maps for as synthesized Cal-P (a-c), Cal-SA-P (d-f) and Cal-FS-P (g-i).

XPS analyses were performed on the proppant samples to determine the chemical composition of the surfaces (Table 2). Fig. 5 shows the normalized Al, Si and Ca content (χ_{Al}, χ_{Si}, and χ_{Ca}, respectively) of pristine proppant compared to the surface of coated proppants, as defined by Eq. 1-3, where Al(at.%), Si(at.%), and Ca(at.%)] are the atomic percentage of each element as determined by XPS (see Table 2).

$$\chi_{Al} = Al(at.\%)/[Al(at.\%) + Si(at.\%) + Ca(at.\%)] \quad (1)$$

$$\chi_{Si} = Si(at.\%)/[Al(at.\%) + Si(at.\%) + Ca(at.\%)] \quad (1)$$

$$\chi_{Ca} = Ca(at.\%)/[Al(at.\%) + Si(at.\%) + Ca(at.\%)] \quad (1)$$

Table 2. XPS analysis (at.%) on the proppant surface for various treatments after synthesis, curing, sintering, and hydration stages.[a]

Sample	Treatment	Ca	Si	Al	C	O
Proppant	None	0.00	11.92	12.22	25.35	49.34
Cal-P	Synthesis	1.08	15.00	10.45	13.60	59.87
	Curing	1.59	8.59	7.38	37.20	35.82
	Sintering	3.48	7.50	5.11	36.42	36.94
	Hydration	7.16	9.40	2.51	27.50	53.43
Cal-SA-P	Synthesis	1.36	16.28	8.83	17.75	55.79
	Curing	1.12	17.32	7.40	14.51	59.65
	Sintering	6.76	9.74	6.66	27.72	48.83
	Hydration	1.40	7.65	5.92	35.76	45.21
Cal-FS-P	Synthesis	1.04	17.27	8.07	18.48	55.14
	Curing	1.21	19.22	4.28	20.03	55.25
	Sintering	9.39	8.32	5.58	21.22	55.49
	Hydration	6.61	7.83	4.95	47.13	33.49

[a] Summary of sample abbreviations provided in Table 1.

Submitted to *Colloids Surf., A.*

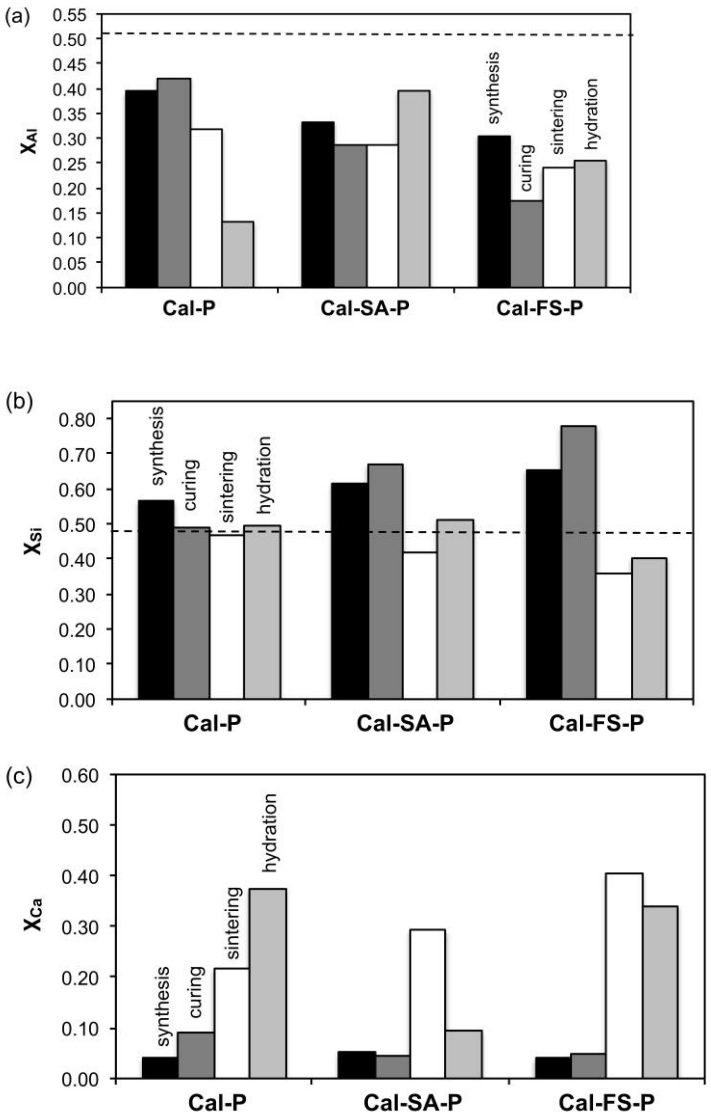

Fig. 5. Normalized relative (a) Al, (b) Si and (c) Ca atomic concentrations as determined by XPS analysis of the surface of coated proppants Cal-P, Cal-SA-P and Cal-FS-P.

The thickness, compactness, and uniformity of the coatings are inversely proportional to the relative Al signal, which is lowered when the coatings are thicker and more compact. In contrast, the Ca and Si concentrations are related to the chemical composition of the materials that cover the proppant. The surface of the untreated proppant is confirmed to be an alumina silicate material with a slightly silicon rich composition (Al:Si = 0.95) as compared the bulk material (Al:Si = 1.02). It is worth noting that coating the proppant with purely $CaCO_3$ (Cal-P) appears to result in a small but significant increase in the Si content as compared to the untreated proppant. This would further suggest a silicon rich surface of the base proppant,

since the addition of a coating lowers the Al detection but not the Si. From the data in Fig. 5a, it is evident that the Al concentration decreases with each of the treatments, consistent with the change in surface morphology and the EDX analysis. Comparing Cal-SA-P and Cal-FS-P, there is a difference in the nature of their coatings, being both of them rich in Si, though with a higher Ca concentration in Cal-SA-P. As a matter of fact, the Ca concentration of Cal-SA-P is the highest among all samples, so we propose that the use of silicic acid seems to favour the adhesion of $CaCO_3$ to the proppant surface.

High-resolution Ca 2p and C 1s XP spectra are consistent with $CaCO_3$, while the Si 2p spectra are typical of silica rather than silicate phases [23]. This chemical characterization is consistent with XRD analysis that shows the as synthesized powders (see below) and the excess powder obtained dislodged from the proppant surfaces (Fig. 6) comprise of crystalline $CaCO_3$ (calcite polymorph, JCPDS 83-1762) [27]. In addition to the crystalline phase of $CaCO_3$ common to all samples, the XRD patterns of the excess powders dislodged during the coating of the proppant particles (Fig. 6b) show a very broad peak of low intensity at about 30° corresponding to an amorphous phase. Based on the peak position and the presence in the non-silica containing sample (Cal-P) we propose that this is due to excess powdered $CaCO_3$ formed by the grinding motion of the proppant during the coating process.

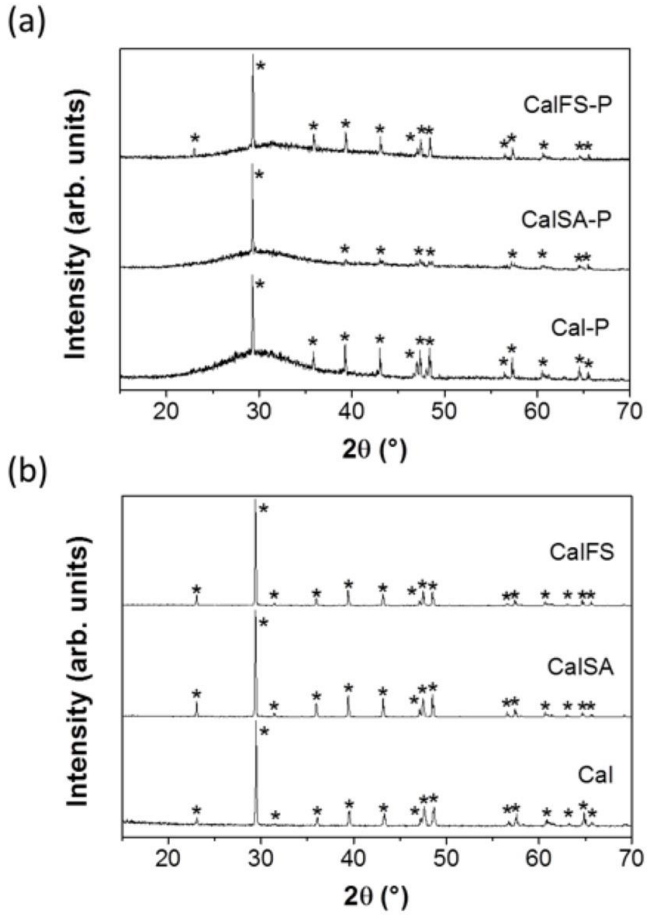

Fig. 6. XRD patterns of (a) Cal, Cal-SA, and Cal-FS powders and (b) Cal-P, Cal-SA-P and Cal-FS-P excess powders dislodged from the proppant surfaces, as listed in Table 1. Peaks are shown for calcite $CaCO_3$ (JCPDS 83-1762).

Confirmation of the XRD results is obtained from FT-IR analyses. Fig. 7 shows the FT-IR transmittance spectra of both the as synthesized free powders and the excess powder obtained dislodged from the proppant surfaces. In all the spectra, the characteristic absorption bands of calcite are observed, including: the OCO in-plane bending mode (ν_4) at around 720 cm^{-1}, the CO_3 out-of-plane bending mode (ν_2) at around 870 cm^{-1}, the asymmetric CO stretching mode (ν_3) at around 1450 cm^{-1}, and the combined modes $\nu_1+\nu_4$ and $\nu_1+\nu_3$ at around 1800 cm^{-1} and 2500 cm^{-1}, respectively [27,28]. The broad absorption band centred at around 1090 cm^{-1} is only observed in the case of the samples Cal-SA, Cal-FS, Cal-SA-P and Cal-FS-P (i.e., samples prepared in the presence of a Si reagent), and it is associated with the SiO_4 tetrahedra stretching mode [30].

Submitted to *Colloids Surf., A.*

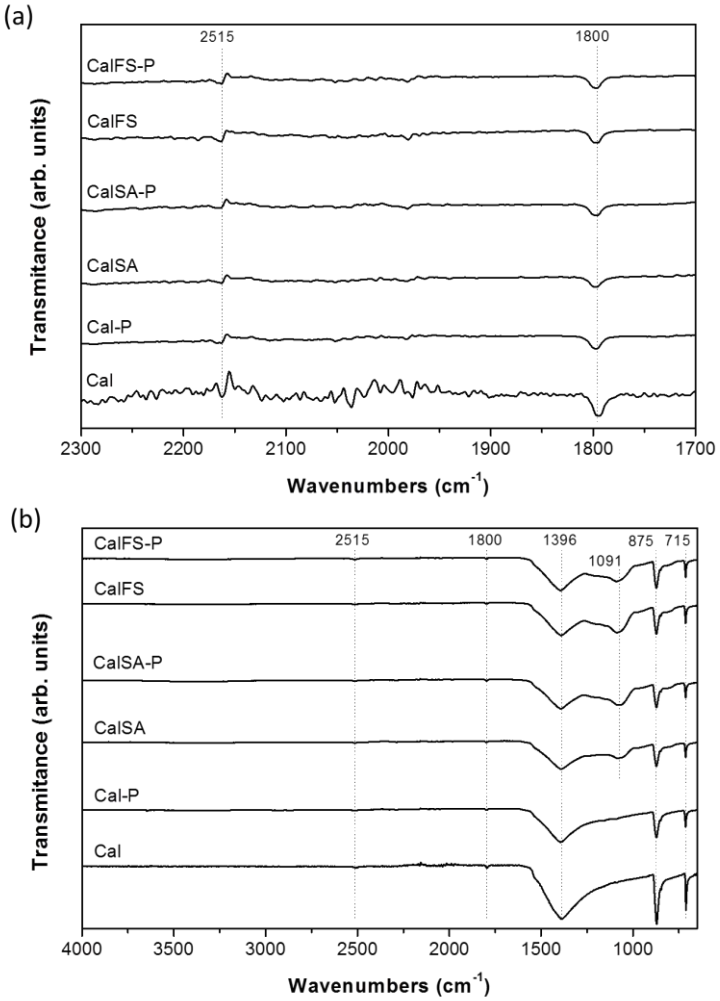

Fig. 7. FT-IR transmittance spectra of Cal, Cal-SA, and Cal-FS powders and Cal-P, Cal-SA-P and Cal-FS-P excess powders dislodged from the proppant surfaces, as listed in Table 1. An expanded view of the spectra between 2300 – 1700 cm^{-1} is shown in (b).

As noted above, samples were prepared in the absence of proppant to determine the interaction of the coating reagents in the absence of the surface. SEM images of these powders show the rhombohedral shape consistent with the calcite phase of $CaCO_3$ (Fig. 8). From a comparison of the morphologies of Cal, Cal-SA and Cal-FS, it appears that effect of the Si reagents is to induce the formation of larger-sized particles during the synthesis. The average particle size of Cal, Cal-SA and Cal-FS are 2.13, 3.50 and 5.80 μm, respectively. It should be noted that while the particle size of fumed silica is 7 nm, we have previously

observed that nanoparticles are able to significantly alter the morphology and crystal phase of $CaCO_3$ precipitates from aqueous solution [31]. The alteration in the particle size observed in the powders is consistent with the change in surface roughness observed for the proppant particles (Fig. 3). Furthermore, comparing the three images in Fig. 8, it is possible to observe how the morphology of the sample Cal-FS is mostly different to the morphology of the samples Cal and Cal-SA, so fumed silica seems to affect the reaction conditions to a greater extent than silicic acid. However, as noted above the effect of Si reagents is localises to certain parts of the bulk of the materials, and this is replicated in the powders. For example, the difference in composition for different features is readily seen in Fig. 9, which shows the EDX analysis for two types of features within a sample.

3.2. Curing

The coated proppant samples (Cal-P, Cal-SA-P, and Cal-FS-P) were subjected to a cure step in water to determine if there is any change in the surface morphology. In addition, both the excess powders of from the proppant syntheses and the powders obtained in the absence of proppant (Cal, Cal-SA and Cal-FS) were studied to facilitate characterization.

As may be seen from the SEM images in Fig. 3, the surface morphology of Cal-P shows an increased in the texture after curing for 7 days (Fig. 3c), as compared to the as-synthesized sample (Fig. 3b). This alteration in texture is consistent with the XPS data (Fig. 5). The small increase in the Al content and concomitant decrease in Si are typical of re-exposing the underlying proppant surface, while the increase in Ca suggests the formation of islands and or grain growth [16].

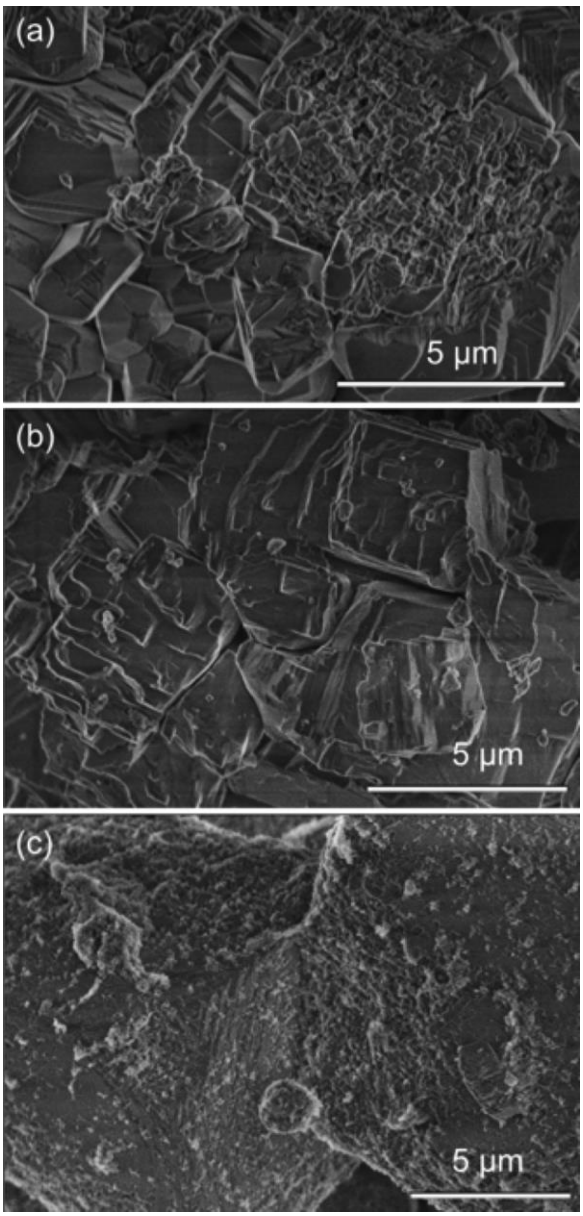

Fig. 8. SEM images of the samples (a) Cal, (b) Cal-SA and (c) Cal-FS, as listed in Table 1, synthesized without proppant.

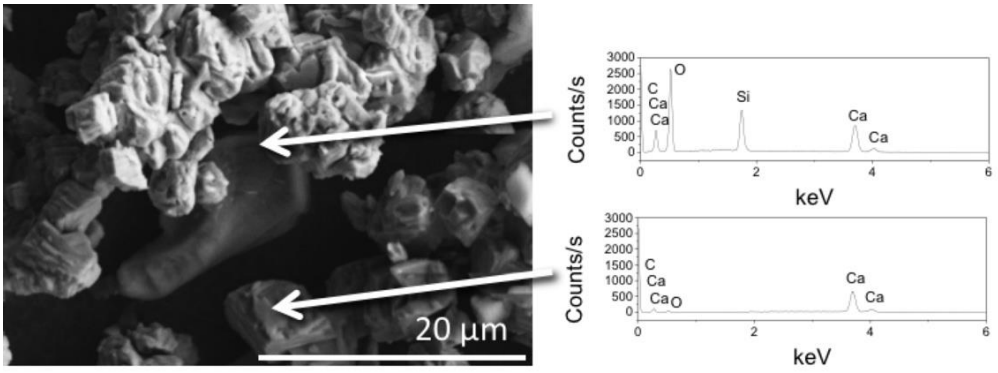

Fig. 9. SEM and EDX spectra for different particles within as synthesized Cal-SA.

In contrast to the surface reorganization of Cal-P, the surface of Cal-SA-P appears little changed visually (see, Fig. 3f and g). However, EDX map of the surface of Cal-SA-P after curing (Fig. 10) appears to show a slight increase in the inhomogeneity of the coating (c.f., Fig. 4). This inhomogeneity increase may be explained by observation of the SEM and associated EDX for Cal-SA sample (Fig. 11). By comparison with the data in Fig. 9, it is clear that upon curing there appears almost a separation of the $CaCO_3$ and silica. The samples before and after curing both show clear rhombohedral features whose EDX analysis is consistent with essentially $CaCO_3$. However, after curing the second Si-richer feature shows both an increase in average size and an increase in Si content.

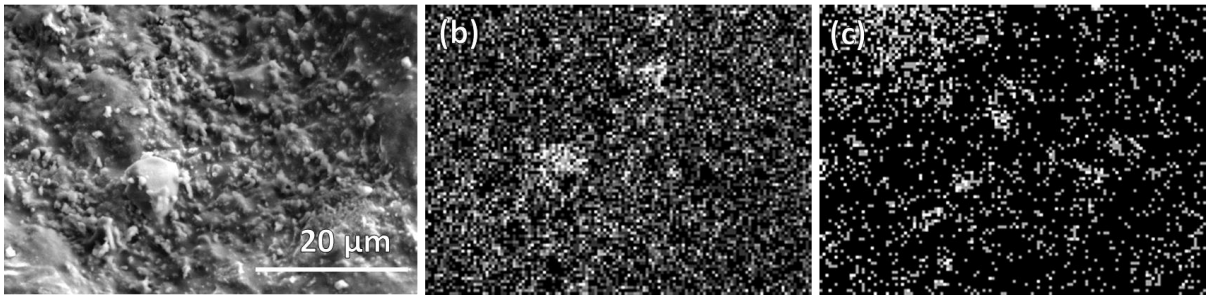

Fig. 10. SEM image (a) and associated Si (b) and Ca (c) EDX maps for Cal-SA-P after curing.

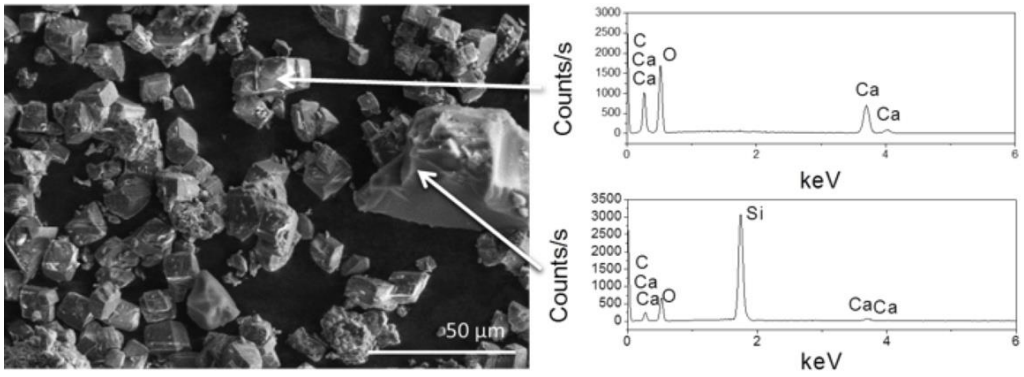

Fig. 11. SEM and EDX spectra for different particles within as cured Cal-SA.

A sample of Cal-SA was cured for 2 months to determine if any chemical speciation changes occurred. As may be seen from Fig. 12, the XRD shows the characteristic sharp diffraction peaks of calcite, but also a broad low intensity feature that is not present before

curing, corresponding to an amorphous phases. Potentially this could be either amorphous Ca_2SiO_4, which diffraction peak is found at around 30° [32] and/or to amorphous $CaCO_3$, with two peaks at 28° and 48° [33]. However, the IR spectra, after curing, show no additional peaks (Fig. 13). Furthermore, the high-resolution Ca 2p and C 1s XP spectra are consistent with $CaCO_3$ and silica, rather than Ca_2SiO_4 [23].

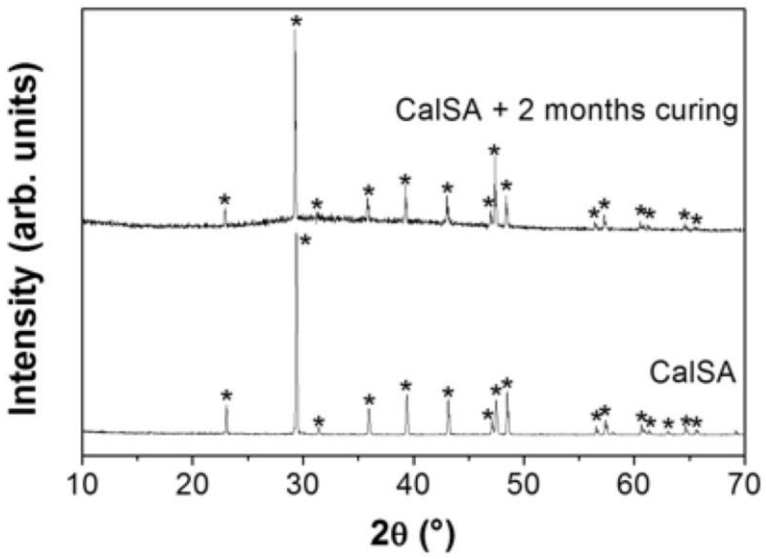

Fig. 12. XRD patterns of Cal-SA powder before and after curing for two months.

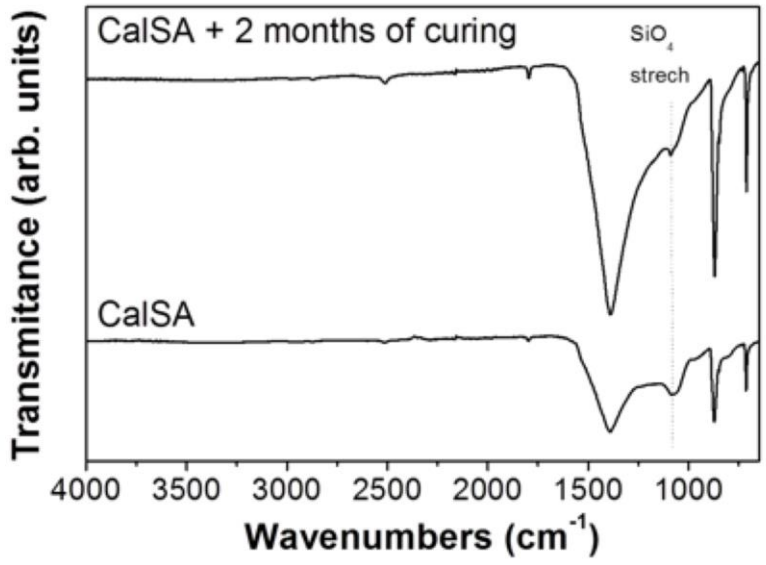

Fig. 13. FTIR transmittance spectra of Cal-SA powder before and after curing for two months.

The SEM images for the surface of Cal-FS-P after curing appears smoother (Fig. 3j and k). The XPS analysis (Fig. 5) shows a marked decrease in the Al content with an increase in Si, but the Ca composition remains essentially unchanged. SEM images of Cal-FS after curing show that Si reagent appears to greatly assist the formation of particle aggregates after curing for 1 week at ambient conditions (Fig. 15). The fumed silica not only favours the growth of large agglomerates during synthesis (Fig. 5c), but also facilitates further agglomeration during the curing process, as previously reported in the literature [34]. However, on the proppant surface it appears to create a more contiguous coating.

The SEM images for the surface of Cal-FS-P after curing appears smoother (Fig. 3j and k). The XPS analysis (Fig. 5) shows a marked decrease in the Al content with an increase in Si, but the Ca composition remains essentially unchanged. SEM images of Cal-FS after curing show that Si reagent appears to greatly assist the formation of particle aggregates after curing for 1 week at ambient conditions. The fumed silica not only favours the growth of large agglomerates during synthesis, but also facilitates further agglomeration during the curing process, as previously reported in the literature [34]. However, on the proppant surface it appears to create a more contiguous coating.

3.3. Sintering

Di-calcium silicate or belite (β-Ca_2SiO_4) is one of the major components of Portland cement clinker. Conventionally, belite is produced by extensive sintering of limestone ($CaCO_3$) and quartz (SiO_2) at temperatures exceeding 1400 °C. Significantly lower temperatures and reaction times are known to be required for the sintering of CaO/SiO_2 mixtures formed through sol-gel synthesis [35,36]. However, it should be noted that where the CaO is present as nanocrystals it has been shown to be resistant to sintering in the presence of silica [37]. In addition, the hydrothermal reaction of fumed silica and lime ($Ca(OH)_2$) has been shown to allow for low temperature synthesis of belite cements [38]. In the attempt to convert the cured materials to a calcium silicate that can undergo hydration and cement formation all the samples were annealed in air at 1200 °C for 1 hour.

As may be seen from the SEM images of the annealed proppant samples (Fig. 3d, h, and l) there is a significant increase in the texture on the surface of the proppants. Images at a higher magnification provide a view of the morphology on the surfaces (Fig. 14). Based upon the SEM images and the associated EDX maps (Fig. 15) it appears that the growth on the surface of Cal-P is enhanced during the decomposition of $CaCO_3$ coating to CaO. In particular, the coating appears to be thicker, an observation supported by the XPS analysis, which shows a decrease in both Al and Si content, but an increase in the Ca content (Fig. 5).

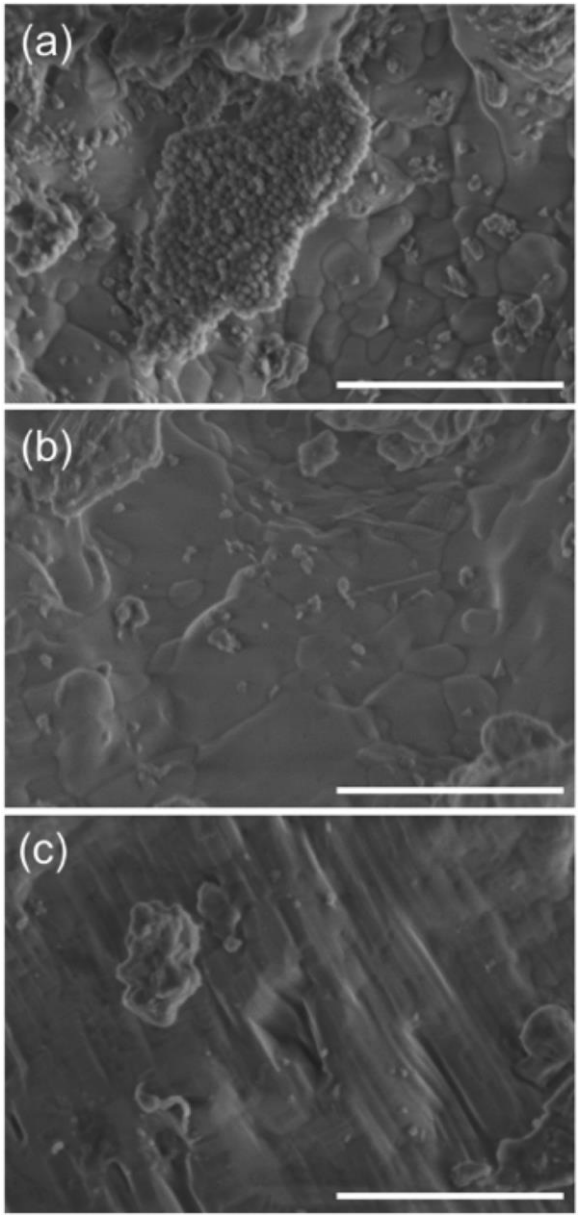

Fig. 14. The SEM images Cal-P (a), Cal-SA-P (b), and Cal-FS-P (c) after sintering at 1200 °C for 1.5 h. Scale bars are 2 μm.

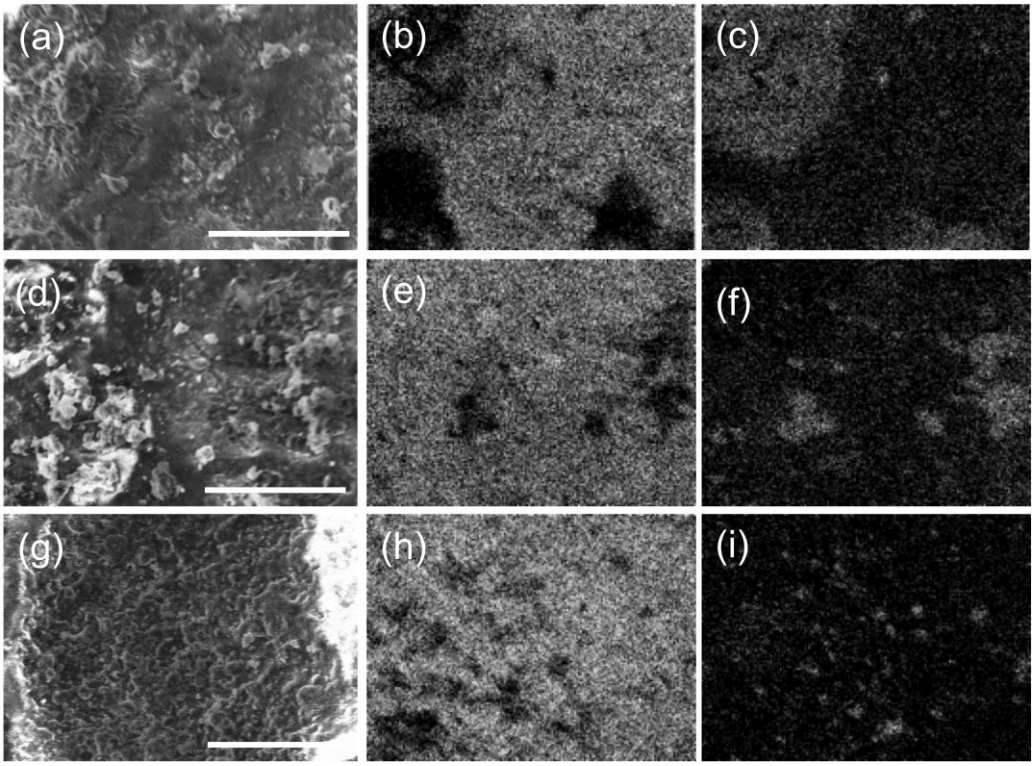

Fig. 15. The SEM images (a-c) and associated Ca (d-f) and Si (g-i) elemental maps for Cal-P (a-c), Cal-SA-P (d-f), and Cal-FS-P (g-i) after sintering at 1200 °C for 1.5 h. Scale bars are 20 μm.

Although the surface morphology of the sintered Cal-SA-P sample (Fig. 14d) looks similar to that of the Cal-P samples (Fig. 14a) the EDX map (Fig. 14e) shows a much more uniform distribution of Ca across the surface. In fact, both Cal-SA-P and Cal-FS-P show a dramatic increase in the Ca content as compared to both Al and Si upon sintering (Fig. 5). The extent of coverage after annealing is entirely dependent on the curing process, such that the proppant particles with the highest covering at the end of the curing (samples Cal-P and Cal-SA-P) were those with the highest volume increase after the sintering.

In order to identify the possible transformations involved in the sintering process, the thermal behaviour of cured Cal, Cal-SA and Cal-FS powders and cured Cal-P, Cal-SA-P and Cal-FS-P coated proppants (in the presence of excess powders) were studied by thermal gravimetric/differential thermal analysis (TG/DTA). The TG/DTA analysis for the Cal-SA, Cal-FS and Cal-FS-P are shown in Fig. 16. In all cases one main endothermic peak was found

at 820-850 °C in correspondence of a large mass decrease due to CO_2 evolution and the conversion of $CaCO_3$ to CaO. In addition, the samples Cal-SA Cal-FS, and Cal-FS-P show an extra shoulder at around 770 °C, related to the transformation of amorphous $CaCO_3$ to CaO [39,40]. The thermograms also confirm the previous hypothesis about the presence of SiO_2 and silicates in the coatings. All the analysis of the samples synthesised without proppant using Si reagents (Cal-SA and Cal-FS), showed a small endothermic transition at about 1065 °C, which could be attributed to the crystallisation of calcium silicate and transition between different calcium silicate crystalline phases [19]. On the other hand, for the samples prepared with proppant (e.g., Cal-FS-P), a different endothermic transition was observed at a lower temperature (see Fig. 16c). This extra transition can be related to the formation of Ca_2SiO_4, as described for cements with $CaO\text{-}SiO_2$ phases in the literature [19].

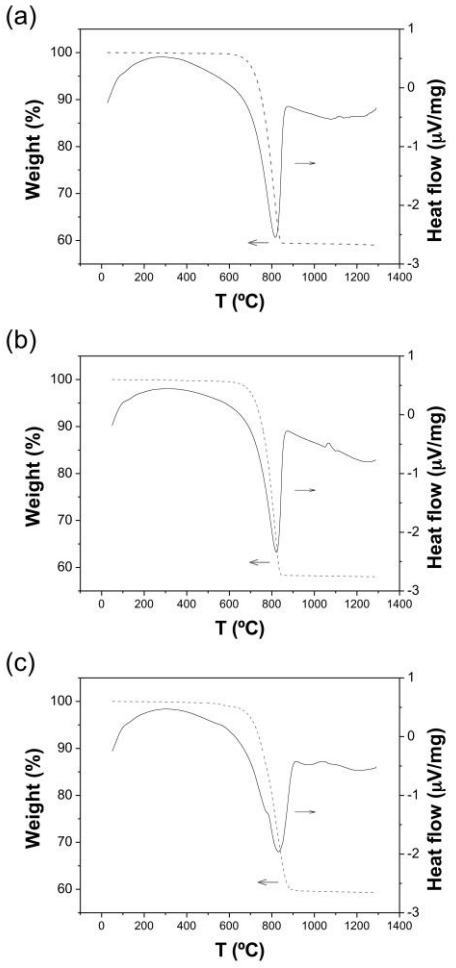

Fig. 16. TG/DTA curves of cured samples (a) Cal-SA, (b) Cal-FS, and (c) Cal-FS-P.

Submitted to *Colloids Surf., A.*

After the thermal treatments, ceramic materials were obtained in all the cases. Above all, after sintering Cal-P, Cal-SA-P and Cal-FS-P the proppant beads were surrounded and linked by ceramic bridges, as shown the SEM pictures presented in Fig. 17a. At the same time, SEM images (Fig. 17b and c) and EDX analysis showed the formation of two kinds of particles after the sintering (1) porous rhombohedral particle aggregates with a Si:Ca average atomic ratio of 0.02 and some dense irregular particles with Si:Ca ratio of 0.58. Also, the SEM images showed that using of Si reagents have a structural effect on the resulting samples. The excess powder is more dense when produces from the sintering of Si containing composites, being much more dense for the samples Cal-FS and Cal-FS-P. This fact demonstrates the importance of using a Si source for the curing process and it reveals once again the adhesive role of Si compounds between different $CaCO_3$ particles (CaO particles after sintering) in the powder.

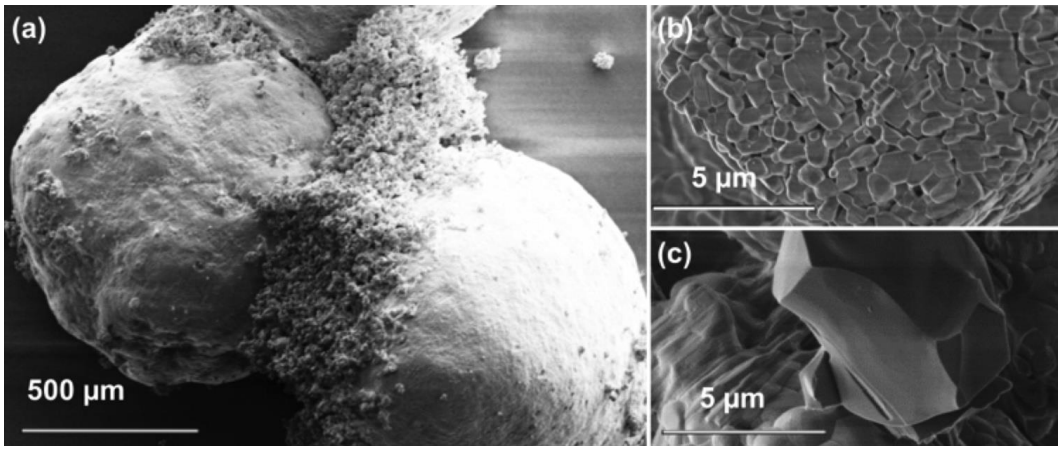

Fig. 17. SEM images of the sample synthesized with proppant, using $CaCO_3$ and H_4SiO_4 as reagents, after the thermal treatment at 1200 °C for 1 hour, at (a) low magnification and high magnification, showing (b) the rhombohedral and (c) the irregular particles.

All materials formed upon sintering were characterised using XRD and FTIR, samples were collected after the thermal treatments at 1200 °C. For example, Fig. 18 presents the XRD pattern of the ceramic excess powder of Cal-SA and part of the coating of Cal-SA-P after thermal treatment. The XRD results showed in both cases the transformation from $CaCO_3$ to CaO after thermal treatment. This fact is supported by the FTIR spectra of the

sintered samples (Fig. 18), where a narrow and intense peak appears at 3645 cm^{-1} and a shoulder at about 1525 cm^{-1}, which are related with the CaO-H stretching and vibration modes, respectively, proper of H_2O molecules or isolated –OH groups adsorbed on the CaO particles [41]. FTIR spectra also revealed the presence of some $CaCO_3$ residues (peaks at 1413, 875 and 715 cm^{-1}), so probably a longer thermal treatment is necessary to quantitatively convert the carbonate to oxide.

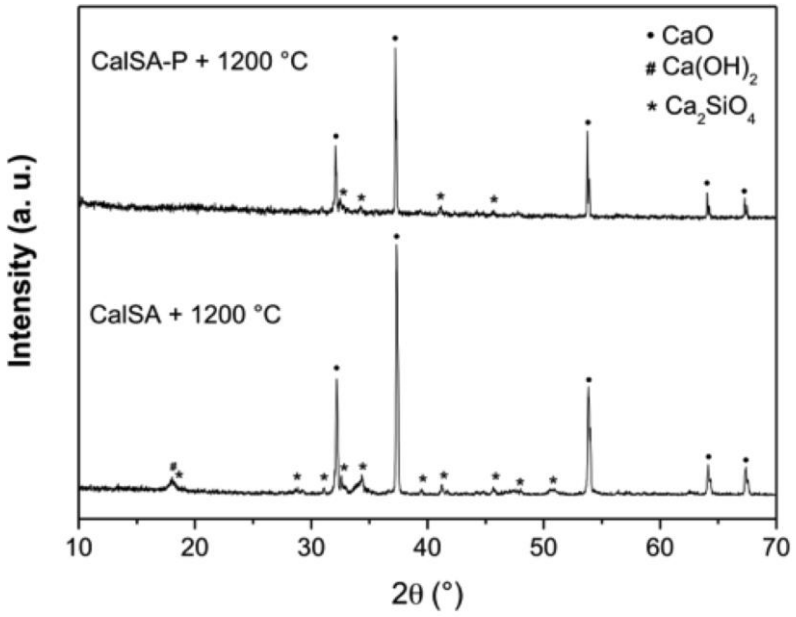

Fig 18. XRD patterns of the Cal-SA and coating materials of Cal-SA-P after thermal treatment at 1200 °C for 1.5 hours.

Ca_2SiO_4 was observed in all samples synthesised with Si reagents (Cal-SA, Cal-FS, Cal-SA-P and Cal-FS-P), both in the XRD patterns (Fig. 18) and the FTIR spectra (Fig. 19), which showed the characteristic peaks of a Ca_2SiO_4 phase (900 and 850 cm^{-1}).[24] In these FTIR spectra there is also a broad absorption band at 1000 cm^{-1} which can be assigned to the stretching mode of SiO_4 tetrahedra, in this case shifted to lower frequency due to the presence of modifier oxide, CaO [30].

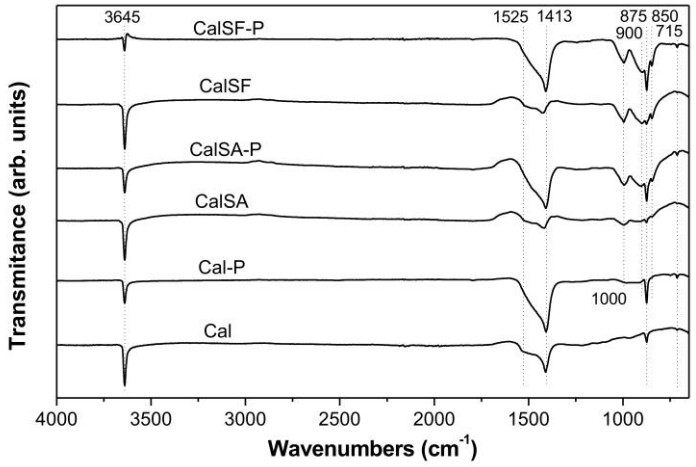

Fig. 19. FTIR transmittance spectra of cured Cal, Cal-SA and Cal-FS powders, and Cal-P, Cal-SA-P, and Cal-FS-P after sintering at 1200 °C.

Beside XRD and FTIR, the surface of the modified proppants were characterised after sintering using XPS, the results are given in Fig. 5. From a direct comparison of the Al concentrations of Cal-P, CalAS-P and Cal-FS-P before and after sintering at 1200 °C (Fig. 5a), it is evident that the coatings of the three samples either became thicker or more compact upon heating since the Al concentration on the surface drops of about 2% in both materials. Furthermore, the sintering of Cal-SA-P and Cal-FS-P produced coatings made with a larger amount of Ca, in this case CaO and $CaSiO_4$ were incorporated to a larger extent in the coatings.

3.4. Hydration

Each of the sintered proppant samples was hydrated for 48 h to observe any morphology changes that would occur once the proppant was 'in-place'. As may be seen from Fig. 3 there is a significant morphological change. In the case of Cal-P (Fig. 3e) there appears to be an increase in the texture of the surface. At higher magnification (Fig. 20) this takes on a popcorn aspect with a crystalline coating on the proppant creating a complex shape. It should be noted that such surface texture would not be amenable for pumping the proppant since these protuberances would likely break of and cause a decrease in conductivity [42]. However, if they were produced in-situ they would presumably be less of an issue. The roundness appears to be only slightly decreased. The sphericity and roundness standard

evaluates the proppant shapes [43]. A lower Krumbein number indicates a more angular proppant. In the case of Cal-P after hydration the roundness appears close to the original base-proppant (0.9). In contrast, the Cal-SA-P and Cal-FS-P samples show a distinct increase in the angularity (0.3 and 0.5, respectively) [43]. But unlike the Cal-P, those with Si appear to create a smooth surface that while misshapen from spherical does not have any sharp features that would be broken of during pumping.

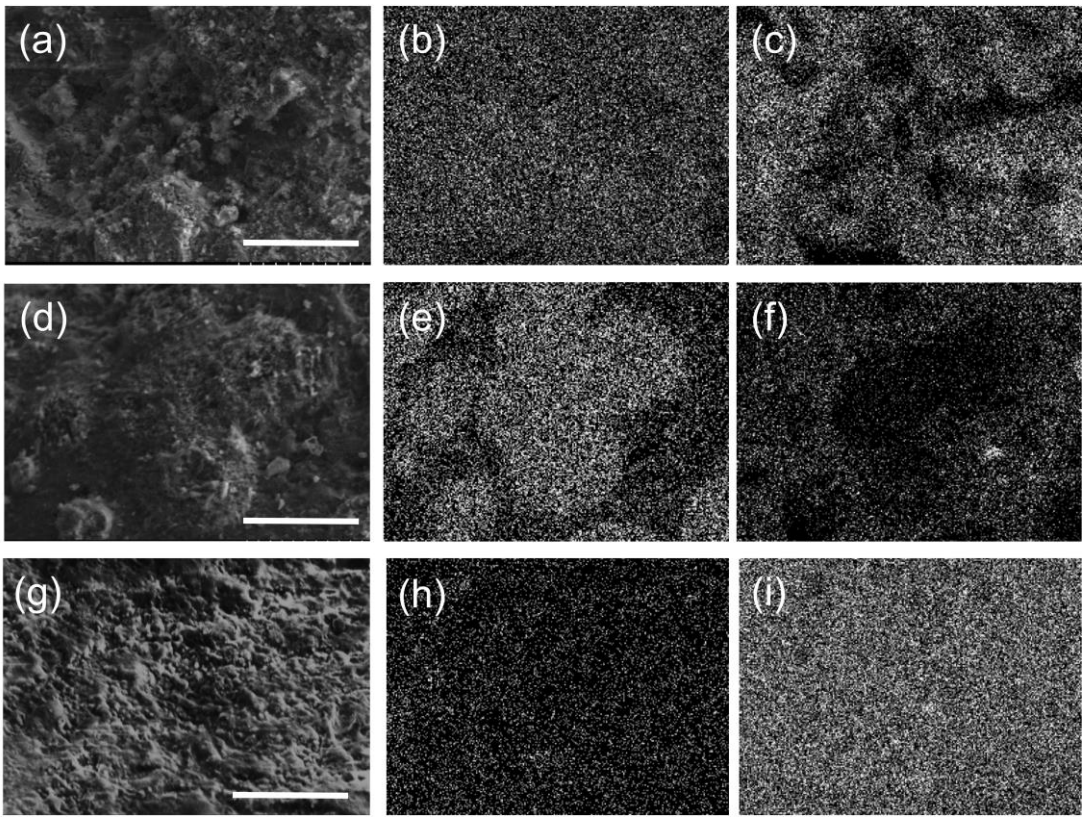

Fig. 19. SEM images (a, d, g) with associated Ca (b, e, h) and Si (c, f, i) EDX map of sintered Cal-P (a-c), Cal-SA-P (d-f) and Cal-FS-P (g-i) after final hydration.

The EDX of the hydrated proppants (Fig. 20) show similar uniformity of distribution of Ca and Si on the surface as compared to the sintered homologs (Fig. 15). However, as is confirmed by XPS (Fig. 5) it appears that in the case of Cal-FS-P there is a reversal in the Ca and Si, in that the Ca decreases in intensity (see, Fig. 19h and i versus Fig. 15h and i).

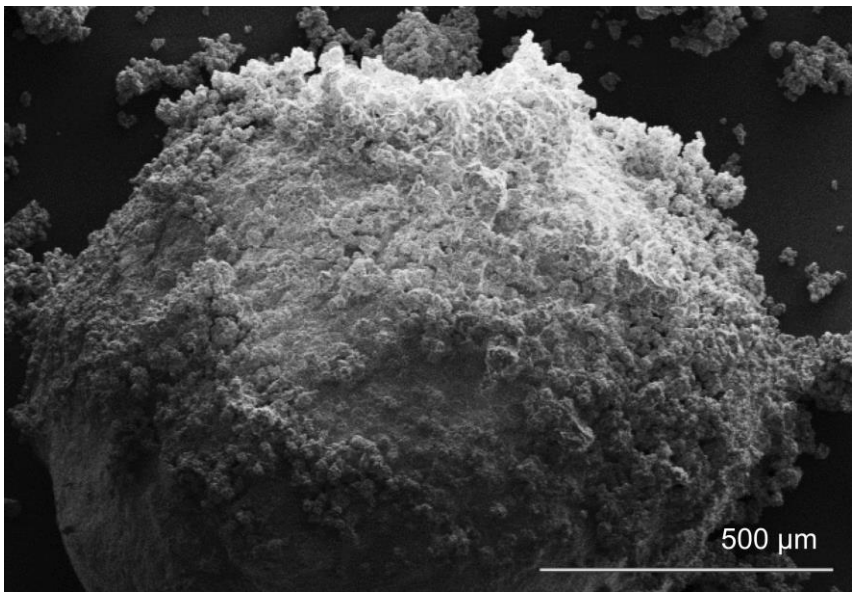

Fig. 20. SEM image sintered Cal-P after final hydration showing the popcorn-like shape at the end of the process.

The above considerations of the effect of synthesis, curing, sintering and hydration on the preparation of coatings and changes in proppant morphology, can be summarised by plotting the change of Si composition (ΔSi, Eq. 4) against the change in the Al composition (Eq. 5), as obtained from the XPS analyses of the samples (Fig. 21). As defined a decrease in the Si (or Al) composition will result in a positive number of ΔSi (or ΔAl). A positive ΔAl signifies an increase in the thickness, density, and contiguous nature of the coating, while the change in the Si content represents the chemical composition of the coatings.

$$\Delta Si = [Si_{Proppant}] - [Si_{Sample}] \quad (4)$$

$$\Delta Al = [Al_{Proppant}] - [Al_{Sample}] \quad (5)$$

In the case of Cal-P samples (Fig. 21a), it is possible to observe that the relative Si content increases slightly for the as synthesized samples, presumably due to the Si-rich surface of the proppant and a non-contiguous coating. Upon curing in water the coating is presumably more uniform (Fig. 3c). Sintering results in the formation of CaO coating that upon hydration gives

a popcorn expansion of the coating (Fig. 3e and Fig. 20) resulting in an increase in the coating thickness and hence decrease in the Al composition.

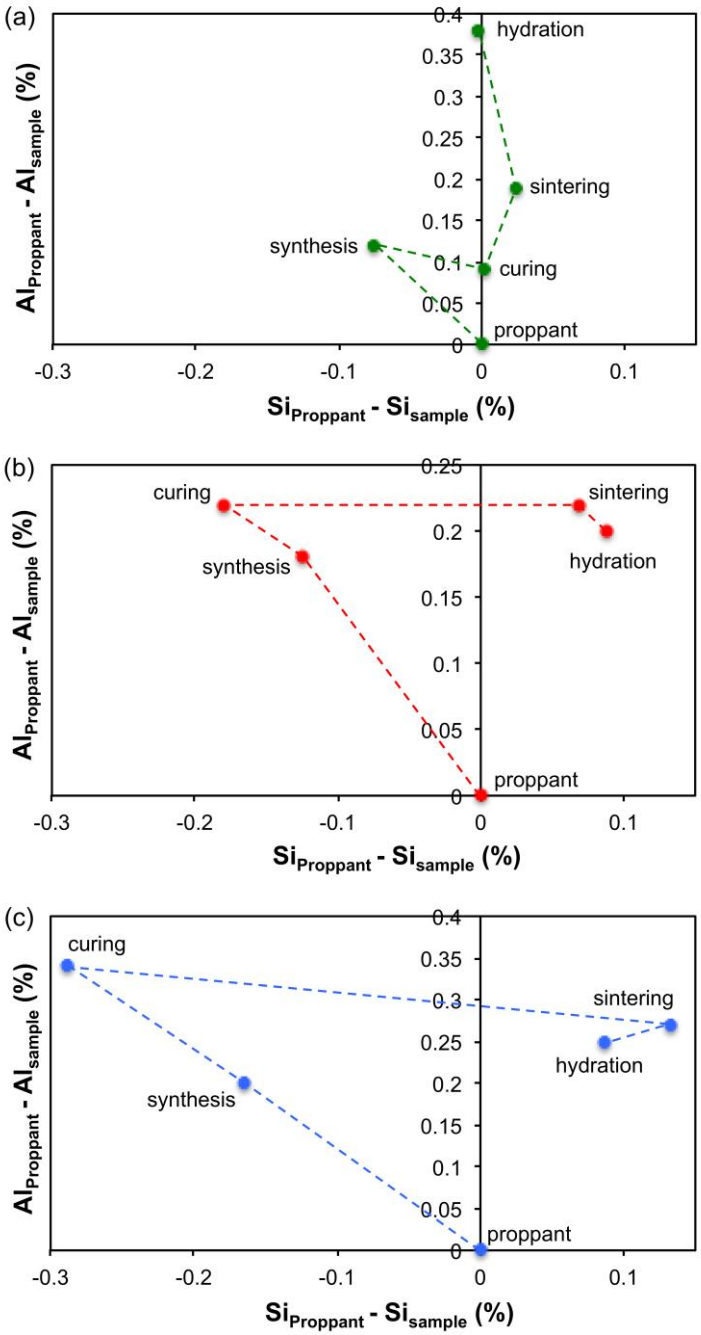

Fig. 21. Plot of the change in Al composition (ΔAl) as a function of the change in Si content (ΔSi) for (a) Cal-P, (b) Cal-FS-P, and (c) Cal-SA-P as a function of chemical/physical transformations.

In the case of Cal-SA-P and Cal-FS samples, synthesis and sintering are the most effective stages, in spite of the negligible increase of amount of coating during curing. On the other hand, a significant change of composition was recorded for Cal-SA-P during this stage with a considerable increase of Si:Ca ratio, probably due to the increase of Ca_2SiO_4 phases in the coating. So, in the presence of Si reagents the preparation process favours the formation of $CaCO_3$/Ca_2SiO_4 rich coating, making the synthesis and sintering steps more effective. The Si composition is increased upon synthesis and curing (negative ΔSi) due to the presence of the Si reagent. Upon sintering the surface Si composition is decreased (positive ΔSi) consistent with a more homogeneous Ca_2SiO_4 containing coating (Fig. 18). It is interesting, however, that for both Cal-FS-P and Cal-SA-P there is only small changes in the surface composition during hydration. This is despite significant morphological changes (Fig. 3).

4. Conclusions

In summary, aluminosilicate proppant particles can be successfully coated with calcite-rich layers following a sol-gel style synthesis approach in water. The use of Si reagents during the synthesis increases the particle size and the adherence of the coatings to the proppant, in particular thicker and more compact coatings are obtained in the presence of fumed silica. Curing in water facilitates the agglomeration of $CaCO_3$ on the coatings, although the coatings formed in the presence of Si reagents did not grow as much as when $CaCO_3$ is used alone. This is due to a competitive adhesion of SiO_2 in place of $CaCO_3$ on the surface of the proppant. Furthermore, when the proppant is cured in the presence of both $CaCO_3$ and silicic acid the resulting coatings undergo a significant compositional change. Sintering allow for the conversion of the cured samples to ceramic agglomerates with the desired “popcorn” shapes. In this case, the coatings and bridges connecting the proppant particles consist of a mixture of CaO and Ca_2SiO_4 ceramic particles. During the sintering step, the thickness and compactness of the coatings increase in all samples. Among all samples, best results are obtained in the presence of Si products, especially Ca_2SiO_4. Finally, hydration of the coated proppants (Cal-FS-P and Cal-SA-P) does allow for a distinct increase in the angularity, which

is the desired transformation to allow the proppant to be locked-in-place once located in the reservoir.

Acknowledgment

This research was supported by the Welsh Government Sêr Cymru Programme, the Sêr Cymru National Research Network in Advanced Engineering and Materials (NRN-141), the Robert A. Welch Foundation (C-0002), and King Saud University. The Authors thank Dr. Cecile Charbonneau (SPECIFIC, Swansea University) for the use of the XRD analysis. The authors declare no competing financial interests.

References

[1] D. Warlick, Gas shale and CBM development in North America. Oil Gas Finance J. 3(2006) 1.

[2] D. Mader, Hydraulic proppant fracturing and gravel packing. New York: Elsevier Science; 1989.

[3] G.E. King, *SPE Annual Technical Conference, Florence, Italy*, September 19-22, 2010; Abstract SPE 133456.

[4] G.T. Tellez, N. Nirmalakhandan, *Produced Water: Technological/Environmental Issues and Solutions*, Eds. J. P. Ray, F. R. Englehardt, Plenum, New York, pp 522-523.

[5] A.R. Barron, A frac-tious issue. Public Service Review: European Union 24 (2012) 252-253.

[6] H. Frasch, Increasing the flow of oil-wells. US Patent 556669 A, March 17 (1896).

[7] M.C. Kulkarni, O.O. Ochoa, Mechanics of light weight proppants: A discrete approach, Compos. Sci. Technol. 72 (2012) 879-885.

[8] B.T. Dewprashad, J.D. Weaver, P.D. Nguyen, M. Parker, M. Blauch, Modifying the proppant surface to enhance fracture conductivity, Soc. Pet. Eng. (1999) doi:10.2118/50733-MS.

[9] P.D. Ellis, B.W. Surles, Chemically inert resin coated proppant system for control of proppant flowback in hydraulically fractured wells, US Patent 5604184A, 1997.

[10] M.A. Parker, P.D. Nguyen, J.D. Weaver, M. Kalman, M.J.R. Segura, B. F. Slabaugh, D. van Batenburg, G. Glasbergen, Fracturing a portion of a subterranean formation to form a propped fracture; slurrying fracturing fluid and high density plastic particles coated with adhesive, US Patent 7281580 B2 (2007).

[11] E. Barmatov, J. Geddes, T. Hughes, D. Willberg, B. Mackay, Manipulation of flow underground. US Patent 8141637 B2 (2012).

[12] J.D. Weaver, P.D. Nguyen, Placing discrete amounts of resin mixture into a well bore comprising a treatment fluid and allowing the resin mixture to substantially cure and form proppant particles while inside the treatment fluid, US Patent 7541318 B2 (2009).

[13] S. Alexander, C.W. Dunnill, A.R. Barron, Assembly of porous hierarchical copolymers/resin proppants: new approaches to smart proppant immobilization via molecular anchors, J. Colloid Interface Sci. 466 (2016) 275-283.

[14] L. Fu, G. Zhang, J. Ge, K. Liao, P. Jiang, H. Pei, X. Li, Surface modified proppants used for porppant flowback control in hydraulic fracturing, Colloids Surf. A 507 (2016) 18-25.

[15] V. Gomez, S. Alexander, A.R. Barron, Proppant immobilization facilitated by carbon nanotube mediated microwave treatment of polymer-proppant structures. Colloids Surf. A 513 (2017) 297-305.

[16] C. Lupu, R.S. Arvidson, A. Lüttge, A.R. Barron, Phosphonate mediated surface reaction and reorganization: implications for the mechanism controlling cement hydration inhibition, Chem. Commun. (2005) 2354-2356.

[17] S.J. Maguire-Boyle, A.R. Barron, Organic compounds in produced waters from shale gas wells, Environ. Sci.: Processes Impacts 16 (2014) 2237-2248.

[18] H.F. Taylor. *Cement Chemistry*, 2nd ed; Thomas Telford Publishing: London, (1997).

[19] V.S. Ramachandran, R.M. Paroli, J.J. Beaudoin, A.H. Delgado, *Handbook of thermal analysis of construction materials*. William Andrew Publishing: New York (2002).

[20] D. Fragoulis, M.G. Stamatakis, D. Papageorgiou, E. Chaniotakis, The physical and mechanical properties of composite cements manufactured with calcareous and clayey Greek diatomite mixtures. Cement Concrete Comp. 27 (2005) 205-209.

[21] E. Fratini, F. Ridi, S.H. Chen, P. Baglioni, Hydration water and microstructure in calcium silicate and aluminate hydrates, J. Phys. Cond. Mater. 18 (2006) S2467-S2483.

[22] J. Zelic, D. Rusic, D. Veza, R. Krstulovic, The role of silica fume in the kinetics and mechanisms during the early stage of cement hydration. Cement Concrete Res. 30 (2000) 1655-1662.

[23] N. Doostdar, C.J. Manrique, M.B. Hamill, A.R. Barron, Synthesis of calcium-silica composites: A route toward an in vitro model system for calcific band keratopathy precipitates. J. Biomed. Mater. Res. Part A 99A (2011) 173-183.

[24] S.-J. Ding, M.-Y. Shie, C.-Y. Wang, Novel fast-setting calcium silicate bone cements with high bioactivity and enhanced osteogenesis *in vitro,* J. Mater. Chem. 19 (2009) 1183-1190.

[25] S. Blonski, S.H. Garofalini, Atomistic structure of calcium silicate intergranular films in alumina studied by molecular dynamics simulations, J. Am. Ceram. Soc. 80 (1997) 1997-2004.

[26] S. Suda, S. Ichikawa, N. Wada, T. Umegaki, Morphology of calcium carbonate coating on amorphous silicate powder, J. Mater. Sci. 35 (2000) 3023-3028.

[27] Y. Boyjoo, V.K. Pareek, J. Liu, Synthesis of micro and nano-sized calcium carbonate particles and their applications, J. Mater. Chem. A 2 (2014) 14270-14288.

[28] O. Nilsen, H. Fjellvag, A. Kjekshus, Growth of calcium carbonate by the atomic layer chemical vapour deposition technique, Thin Solid Films 450 (2004) 240-247.

[29] B. Xu, K.M. Poduska, Linking crystal structure with temperature-sensitive vibrational modes in calcium carbonate minerals, Phys. Chem. Chem. Phys. 16 (2014) 17634-17639.

[30] G. Laudisio, F. Branda, Sol-gel synthesis and crystallisation of $3CaO•2SiO_2$ glassy powders. Thermochim. Acta 370 (2001) 119-124.

[31] R.E. Anderson, A.R. Barron, Effect of carbon nanomaterials on calcium carbonate crystallization, Main Group Chem. 4 (2005) 279-289.

[32] X.J. Kang, S.S. Huang, P.P. Yang, P.A. Ma, D.M. Yang, J. Lin, Preparation of luminescent and mesoporous Eu^{3+}/Tb^{3+} doped calcium silicate microspheres as drug carriers via a template route, Dalton Trans. 40 (2011) 1873-1879.

[33] A.V. Radha, T.Z. Forbes, C.E. Killian, P. Gilbert, A. Navrotsky, Transformation and crystallization energetics of synthetic and biogenic amorphous calcium carbonate, Proc. Natl. Acad. Sci. U.S.A. 107 (2010) 16438-16443.

[34] M. Georgescu, A. Badanoiu, Hydration process in $3CaO•SiO_2$-silica fume mixtures, Cement Concrete Comp. 19 (1997) 295-300.

[35] A. Meiszterics, K. Sinkó, Sol–gel derived calcium silicate ceramics, Colloid Surface. A 319 (2008) 143-148.

[36] R. Chrysafi, Th. Perraki, G. Kakali, Sol–gel preparation of $2CaO•SiO_2$, J. Eur. Ceram. Soc. 27 (2007) 1707-1710.

[37] A. Prathap, M.M. Shaijumon, K.M. Sureshan, CaO nanocrystals grown over SiO_2 microtubes for efficient CO_2 capture: organogel sets the platform, Chem. Commun. 52 (2016) 1342-1345.

[38] M.A. Tantawy, M.R. Shatat, A.M. El-Roudi, M.A. Taher, M. Abd-El-Hamed, Low temperature synthesis of belite cement based on silica fume and lime, Int. Sch. Res, Notices 2014 (2014) 873215.

[39] M.S. Amin, S.A. Abo-El-Enein, A.A. Rahman, K.A. Alfalous, Artificial pozzolanic cement pastes containing burnt clay with and without silica fume, J. Therm. Anal. Calorim. 107 (2012) 1105-1115.

[40] A. Khmiri, M. Chaabouni, B. Samet, Chemical behaviour of ground waste glass when used as partial cement replacement in mortars, Constr. Build. Mater. 44 (2013) 74-80.

[41] G.S. Pappas, P. Liatsi, I.A. Kartsonakis, I. Danilidis, G. Kordas, Synthesis and characterization of new SiO_2–CaO hollow nanospheres by sol–gel method: Bioactivity of the new system, J. Non-Cryst. Solids 354 (2008) 755-760.

[42] F. Liang, M. Sayed, G. A. Al-Muntasheri, F. F. Chang, L. Li, A comprehensive review on proppant technologies, Petroleum 2 (2016) 26-39.

[43] W.C. Krumbein, L.L. Sloss, *Stratigraphy and Sedimentation* (second ed.), W. H. Freeman and Company, San Francisco (1963), p. 660.